

# Electronic Correlations and Hund's Rule Coupling in Trilayer Nickelate $\text{La}_4\text{Ni}_3\text{O}_{10}$

Zihao Huo<sup>1</sup>, Peng Zhang<sup>2,\*</sup>, Zihan Zhang<sup>1</sup>, Defang Duan<sup>1,\*</sup>, and Tian Cui<sup>3,1</sup>

<sup>1</sup>*Key Laboratory of Material Simulation Methods & Software of Ministry of Education, State Key Laboratory of Superhard Materials, College of Physics, Jilin University, Changchun 130012, China*

<sup>2</sup>*MOE Key Laboratory for Non-equilibrium Synthesis and Modulation of Condensed Matter, Shaanxi Province Key Laboratory of Advanced Functional Materials and Mesoscopic Physics, School of Physics, Xi'an Jiaotong University, Xi'an 710049, China*

<sup>3</sup>*Institute of High Pressure Physics, School of Physical Science and Technology, Ningbo University, Ningbo 315211, China*

\*Corresponding author: duandf@jlu.edu.cn, zpantz@mail.xjtu.edu.cn

**Abstract:** Trilayer Ruddlesden-Popper phase  $\text{La}_4\text{Ni}_3\text{O}_{10}$  has been observed with  $T_c$  over 30 K at high pressure in recent experiment, which further expanded the nickelate superconductors family. In this study, we explored the effects of electronic correlations in  $\text{La}_4\text{Ni}_3\text{O}_{10}$  using density function theory plus dynamical mean-field theory at ambient pressure and high pressure. Our derived spectral functions and Fermi surface of ambient phase are nicely consistent with the experimental results of angle-resolved photoemission spectroscopy, which emphasized the importance of electronic correlations in  $\text{La}_4\text{Ni}_3\text{O}_{10}$ . We also found the electronic correlations in pressured  $\text{La}_4\text{Ni}_3\text{O}_{10}$  are both orbital-dependent and layer-dependent due to the presence of Hund's rule coupling. There is a competition between Hund's rule coupling and crystal-field splitting, where the Ni-O layers with weaker crystal field splitting energy would have stronger electronic correlations.

## I. Introduction

Exploration of high- $T_c$  superconductors has been one of the most important frontiers in condensed matter physics. As the first discovered high- $T_c$  superconductors, cuprates [1-4] have inspired the searches for superconductivity in oxide compounds. Due to the similarities with cuprates, nickelates have long been suggested as candidates of high- $T_c$  superconductors [5-8]. In 2019, a Sr-doped infinite-layer  $\text{NdNiO}_2$  with  $T_c$  of 15 K have been discovery [9]. Following this success, the superconductivity of infinite-layer nickelate have been widely explored [10-14]. Enormous investigations have been carried out concerning the physical properties of this superconducting system, such as the multiorbital nature [15], the Hund's metal behaviors [16], and the Kondo coupling [17-19]. Lately, superconductivity in bilayer Ruddlesden-Popper (RP) phase  $\text{La}_3\text{Ni}_2\text{O}_7$  have been observed with a maximum  $T_c$  of 80 K at pressure above 14 GPa [20-25]. As a second unconventional superconductor family with  $T_c$  higher than the boiling temperature of liquid nitrogen, this breakthrough has attracted extensive attentions related to the superconductivity in  $\text{La}_3\text{Ni}_2\text{O}_7$  [26-37], such as the orbital-selective behavior [33, 38], the Hund's rule coupling [30, 39, 40], and the interlayer superexchange interactions [41, 42]. The orbital-dependent electronic correlations and interlayer interactions have been experimental measured at ambient pressure [36, 37], which may support the interlayer superexchange and multiorbital nature.

Recently, trilayer RP phase  $\text{La}_4\text{Ni}_3\text{O}_{10}$  have been observed with  $T_c$  of  $\sim 30$  K at pressure above 15 GPa [43-47], resulting from a structural transition from the  $P2_1/a$  phase at the ambient pressure to the  $I4/mmm$  phase at high pressure. Besides, some experiments reported that  $\text{La}_4\text{Ni}_3\text{O}_{10}$  possess similar electronic state with  $\text{La}_3\text{Ni}_2\text{O}_7$  and both nickelates have orbital-dependent electronic correlations at the ambient pressure [48, 49]. However, the  $T_c$  of  $\text{La}_4\text{Ni}_3\text{O}_{10}$  is much lower than  $\text{La}_3\text{Ni}_2\text{O}_7$ . The effective model of  $\text{La}_4\text{Ni}_3\text{O}_{10}$  have been proposed [50-54] and suggested that the lower  $T_c$  may due to the weaker hybridization between the  $\text{Ni-}d_{z^2}$  and  $\text{Ni-}d_{x^2-y^2}$  orbitals. Besides, using density function theory plus dynamical mean-field theory (DFT+DMFT), the researchers proposed that the electronic correlation effects at different Ni-O layer are not similar [55, 56]. Therefore, it is important to study the effects of electronic correlations in pressured  $\text{La}_4\text{Ni}_3\text{O}_{10}$  and to explore the origination of layer-dependent electronic correlations.

In this work, we studied the effects of electronic correlations, especially the Hund's rule coupling, in trilayer nickelate  $\text{La}_4\text{Ni}_3\text{O}_{10}$  using the DFT+DMFT method. We found that the electronic structures of ambient phase are consistent with the experimental observations, indicating the important role of electronic correlations. We then studied the high-pressure phase and suggested that the electronic correlations of  $\text{Ni-}d_{z^2}$  orbitals are stronger than these of  $\text{Ni-}d_{x^2-y^2}$  orbitals, presenting an orbital-dependent nature. Besides, the magnitudes of electronic correlations are dependent on the Ni-O layers. Both the orbital-dependent and the layer-dependent features of electronic correlations are originated from the Hund's rule coupling. By analyzing the

evolution of atomic state probability and Hund's rule coupling, we suggested that a competition between the Hund's rule coupling and the crystal field splitting. The Ni-O layer with weaker crystal field splitting energy would have a stronger correlation.

## II. Computational details

We perform fully charge self-consistent DFT+DMFT calculations using the eDMFT package developed by Haule *et al.* [57] with the Wien2k package for the DFT part[58]. The exchange-correlation functional was described using the Perdew-Burke-Ernzerhof exchange-correlation potential [59] and  $11 \times 11 \times 3$   $k$ -points were used in both  $P2_1/a$ - and  $I4/mmm$ -La<sub>4</sub>Ni<sub>3</sub>O<sub>10</sub>. The double counting method in DFT+DMFT was treated using the nominal scheme [57], which was suggested as a suit scheme in the study of La<sub>3</sub>Ni<sub>2</sub>O<sub>7</sub> [30]. The hybridization expansion continuous-time quantum Monte Carlo method (CTQMC) [60-62] is used as the impurity solver of the self-consistent DMFT equation [63]. In each DMFT iteration,  $6 \times 10^8$  Monte Carlo updates are used and the self-energy is derived from Dyson's equation. The converged self-energy from DMFT is used to update the new charge density and the new Kohn-Sham potential for the next DFT calculation. The DFT+DMFT loops iterate until the fully convergence of the charge density, the self-energy and the hybridization functions and so on. The maximum entropy method is used for analytic continuation of the self-energy from the imaginary frequency to the real frequency [64]. We choose the on-site Hubbard  $U = 4$  eV and the Hund's rule coupling  $J = 1$  eV to parameterize the electron correlations in the Ni-3d orbitals. Additionally, several different alternative Hubbard  $U$  and Hund's rule coupling  $J$  ( $U = 4$  eV,  $J = 0.5$  eV and  $U = 2$  eV,  $J = 1$  eV) have been tested, as shown in Fig. S1 and S2 of Supplemental Material.

## III. Results and discussion

La<sub>4</sub>Ni<sub>3</sub>O<sub>10</sub> has a monoclinic  $P2_1/a$  symmetry at the ambient pressure, which can be termed as an inter-growth of three NiO<sub>6</sub> octahedra planes and two La-O fluorite-type layers stacking along the  $c$  directions. We adopted the crystal structure from previous experimental data [44] and calculated its band structures and density of states (DOS) using DFT+ $U$  method, as shown in Fig. 1(a). An effective  $U = 3.5$  eV is employed in the correlated Ni-3d orbitals, in line with previous bilayer and trilayer nickelate works [37, 53]. Our results show that both the Ni- $d_{z^2}$  and Ni- $d_{x^2-y^2}$  orbitals cross the Fermi level ( $E_F$ ), which is different from bilayer *Amam*-La<sub>3</sub>Ni<sub>2</sub>O<sub>7</sub> at the ambient pressure with only Ni- $d_{x^2-y^2}$  orbitals cross the  $E_F$  [37]. There are two pockets around the  $\Gamma$  point in Fig. 1(c), including a smaller electronic  $\gamma$  pocket and a relatively larger electronic  $\alpha$  pocket. Our DFT derived Fermi surface is similar to those reported in previous DFT calculations [45, 48], however being contradicted with the angle-resolved photoemission spectroscopy (ARPES) results [45, 48], where only one pocket around the  $\Gamma$  point is observed. We then calculated the  $k$ -resolved spectral

functions and DOS at 100 K using DFT+DMFT method, as plotted in Fig. 1(b). Compared to DFT result, both the  $\alpha$ ,  $\beta$ , and  $\gamma$  bands are strongly renormalized and become very flat near the  $E_F$ . The energy range of Ni- $d_{z^2}$  and Ni- $d_{x^2-y^2}$  DOS are only about 0.2 eV, a factor of about 3.5 times narrower than the DFT result. Besides, for energy below -0.2 eV, the spectral functions become more incoherent due to the strong electronic interaction, which is also consistent with the ARPES results. It is noticed that the  $\gamma$  band does not cross the  $E_F$ , therefore the  $\gamma$  pocket vanished after electron-electron scattering and multi-orbital coupling are included by DMFT. As shown in Fig. 1(d), there is only one electronic  $\alpha$  pocket in octagon shape around the  $\Gamma$  point in the eDMFT derived Fermi surface, which nicely overlap with the APRES results. Both the spectral functions and the derived Fermi surface indicate that DFT+DMFT method can provide improved description of  $\text{La}_4\text{Ni}_3\text{O}_{10}$  than DFT by comparison with experimental results. It means that the DFT picture in this system is insufficient due to the strong electronic correlations of Ni- $d$  electrons. The consistency between our DFT+DMFT calculations and the ARPES results thus emphasized the importance of electronic correlations in  $\text{La}_4\text{Ni}_3\text{O}_{10}$ , and justified our choice of Hubbard  $U = 4$  eV and Hund's rule coupling  $J = 1$  eV in this work.

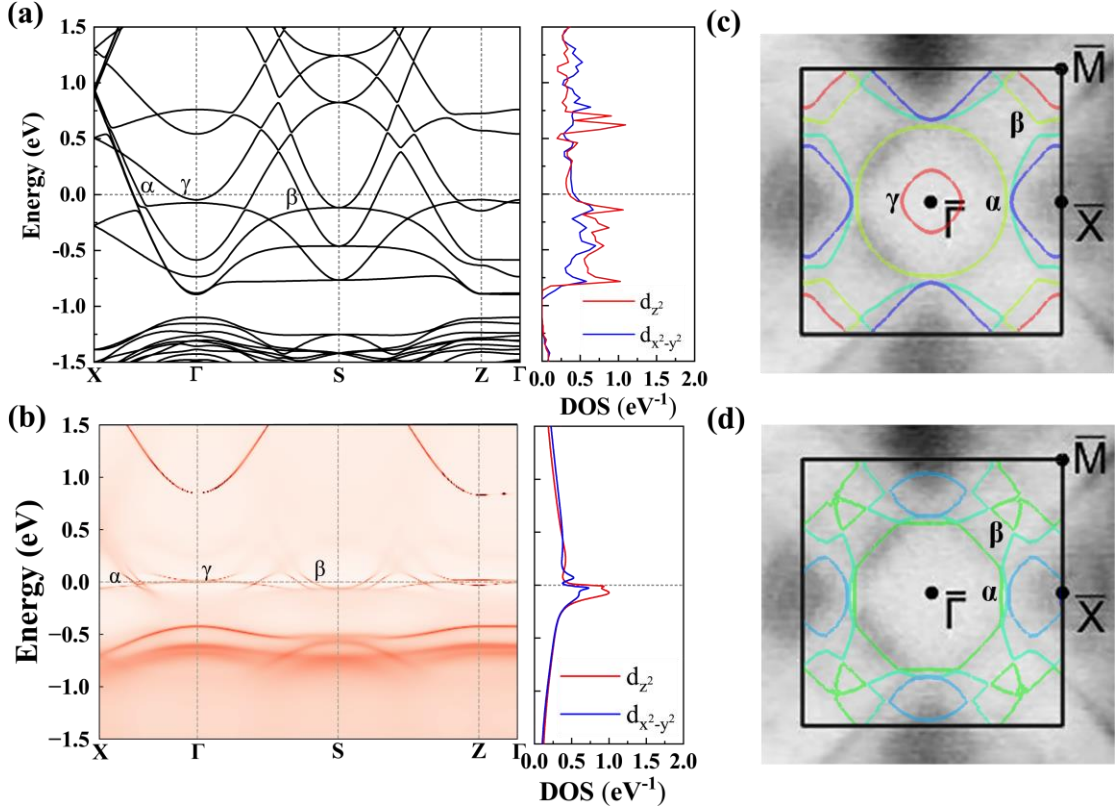


FIG 1. (a) Electronic band structures and DOS of the  $P2_1/a$  phase calculated by DFT+ $U$  ( $U = 3.5$  eV). (b)  $k$ -resolved spectral functions and DOS of the  $P2_1/a$  phase calculated by DFT+DMFT at 100 K. The horizontal gray dashed line represents the Fermi level. (c-d) Fermi surface mapping from Zhang *et al.*'s research [45], and colored solid lines represent two-dimensional Fermi surface of the  $P2_1/a$  phase

calculated by DFT+ $U$  and DFT+DMFT at 100 K, respectively. Different colors represent different band index.

Next, we studied the  $\text{La}_4\text{Ni}_3\text{O}_{10}$  at pressure of 30.5 GPa, which adopts a tetragonal symmetry (space group:  $I4/mmm$ ) (Fig. 2(a)) with lattice parameters  $a = 3.709 \text{ \AA}$  and  $c = 26.716 \text{ \AA}$  [44]. We define the upper and lower Ni-O layers as the outer layers and the middle Ni-O layers as the inner layers. Fig. 2(b-e) represent the DOS and the hybridization functions of Ni- $d_{z^2}$  and Ni- $d_{x^2-y^2}$  orbitals at 100 K. For the inner layer, we can see that both the DOS of Ni- $d_{z^2}$  and Ni- $d_{x^2-y^2}$  orbitals formed a peak near the  $E_F$ . It suggests that Ni- $d_{z^2}$  and Ni- $d_{x^2-y^2}$  orbitals producing characteristic quasiparticle spectra peaks in the inner layers. The existence of high hybridization peaks of Ni- $d_{z^2}$  and Ni- $d_{x^2-y^2}$  orbitals at around 0.3 eV in Fig. 2(d) indicated that these two orbitals have strong hybridization with the O- $p$  orbitals. The strength of hybridization peak of Ni- $d_{z^2}$  and Ni- $d_{x^2-y^2}$  orbitals in the outer layers at around 0.3 eV is lower than the inner layer, which indicate that the hybridization strength of these two orbitals in outer layer is weaker than these in inner layers.

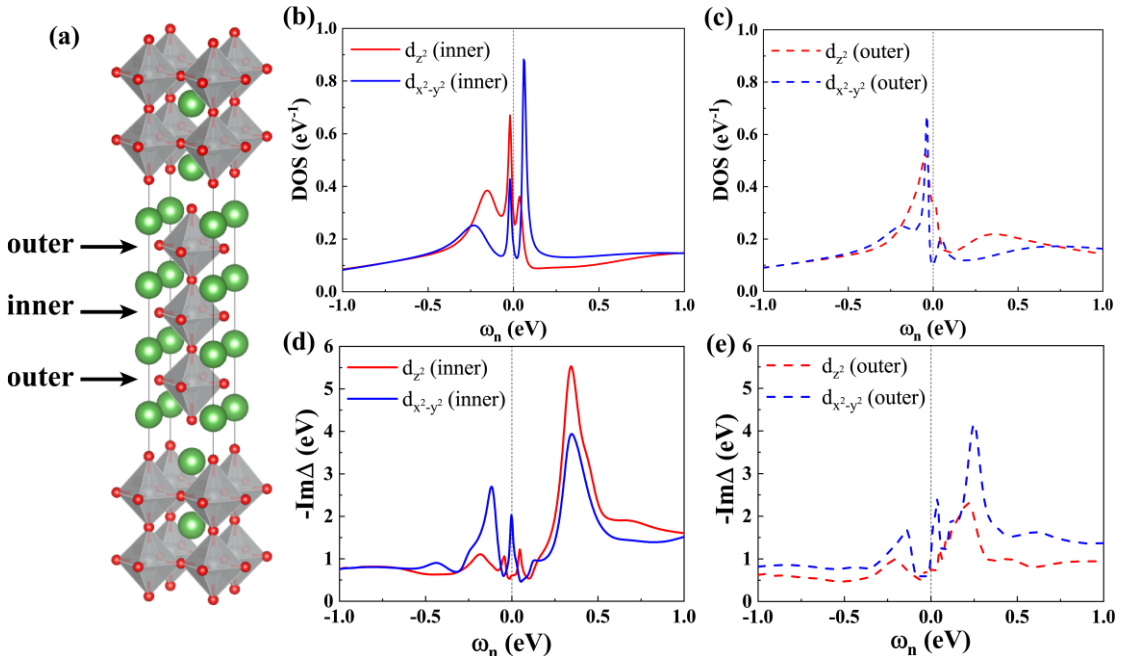


FIG. 2. (a) Crystal structures of the trilayer RP phase  $I4/mmm$  phase. The green, grey, and red spheres represent La, Ni, and O atoms, respectively. Orbital-dependent electronic DOS of Ni in (b) inner and (c) outer layer in  $I4/mmm$  phase at 100 K. The grey dashed line indicated the Fermi level. The pseudo gap is plotted in the inset of (b). (d-e) Negative of the imaginary part of hybridization function at 100 K.

We then calculated the imaginary parts of the Matsubara-frequency self-energy functions in Fig. 3(a) to further analyze the strength of electronic correlations of Ni- $d_{z^2}$  and Ni- $d_{x^2-y^2}$  orbitals. We can find that the imaginary part of self-energy functions

$\text{Im} \sum (i\omega_n)$  of these two orbitals in both inner and outer layers extrapolate to zero as

$\omega \rightarrow 0$ , which suggests the coherent electron-scattering in  $\text{La}_4\text{Ni}_3\text{O}_{10}$  at 100 K. In both the inner and the outer layers, the self-energy function magnitudes of Ni- $d_{z^2}$  orbitals are larger than those of Ni- $d_{x^2-y^2}$  orbitals, which indicates the quasi-particle

weight  $Z = \left[ 1 - \frac{\partial \text{Im} \sum (\omega_n)}{\partial \omega_n} \right]^{-1} \Big|_{\omega_n \rightarrow 0^+}$  of the Ni- $d_{z^2}$  orbitals would be smaller. Since

the quasiparticle weight  $Z$  is parameterized to measure the strength of electronic correlation, in that the value of  $Z$  is inversely proportional to the strength of electronic correlations. Therefore, the correlation strength of the Ni- $d_{z^2}$  orbitals would be larger than that of the Ni- $d_{x^2-y^2}$  orbitals. Our discovery of the orbital-dependent electronic correlation feature and stronger correlated Ni- $d_{z^2}$  orbitals in  $I4/mmm$  phase of  $\text{La}_4\text{Ni}_3\text{O}_{10}$  is consistent with previous experimental observation at ambient pressure[48]. Similarly, the self-energy magnitudes of Ni- $d_{z^2}$  and Ni- $d_{x^2-y^2}$  orbitals in outer layers are always larger than these in inner layers. Following the same logic, we argue the correlation effects of the outer layer is stronger than these of the inner layers, and  $I4/mmm$  phase of  $\text{La}_4\text{Ni}_3\text{O}_{10}$  presents a layer-dependent electronic correlations feature.

Since the Hund's rule coupling  $J$  have been suggested important in pressured  $\text{La}_3\text{Ni}_2\text{O}_7$  [30], we examined the effects of Hund's rule coupling by setting  $J = 0$  eV. The imaginary parts of the Matsubara-frequency self-energy functions with  $U = 4$  eV and  $J = 0$  eV have been plotted in Fig. 3(b). Either the orbital dependent diversity or the layer dependent diversity have been strongly quenched in comparison with the self-energies of  $U = 4$  eV and  $J = 1$  eV in Fig. 1a, which suggests the orbital-dependent and layer-dependent electronic correlation is mainly due to the Hund's rule coupling.

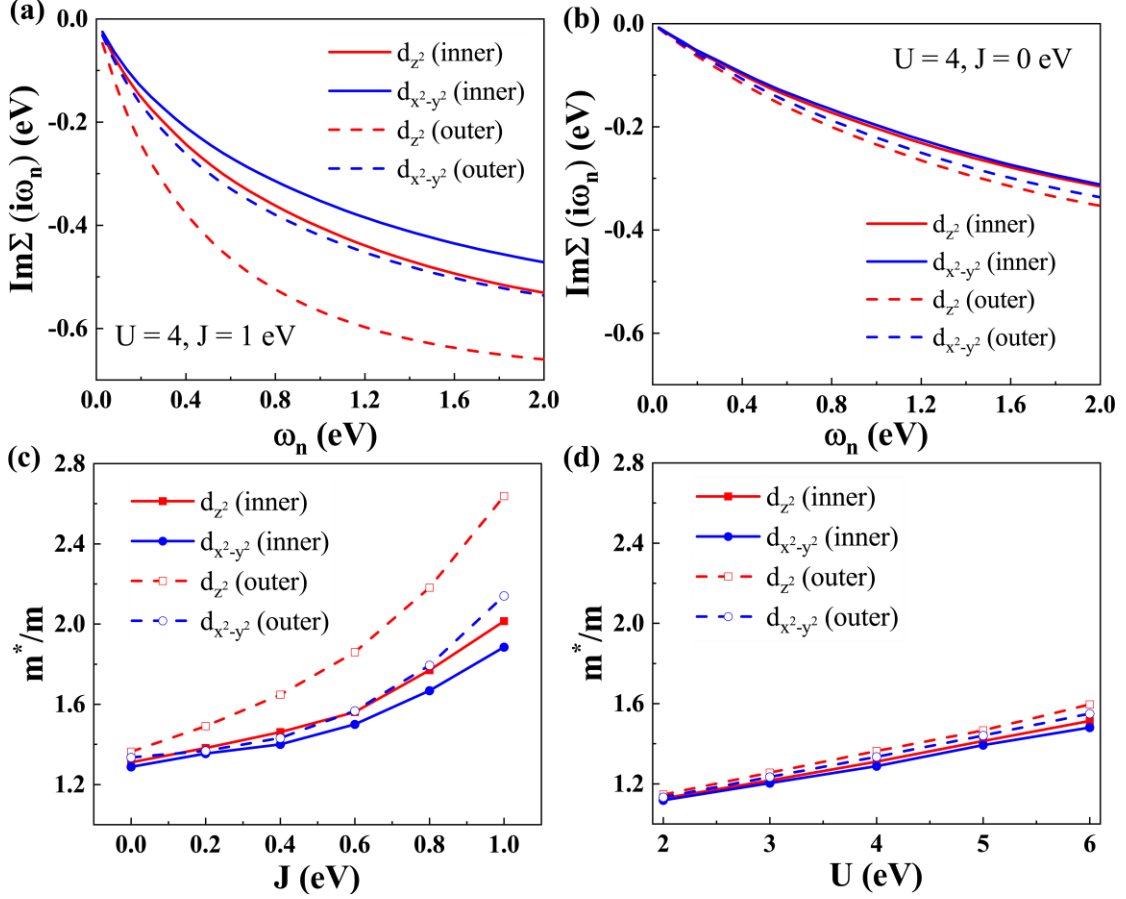


FIG 3. Imaginary parts of the orbital-dependent self-energy functions  $\text{Im}\Sigma(i\omega_n)$  for (a)  $U = 4$ ,  $J = 1$  eV and (b)  $U = 4$ ,  $J = 0$  eV on the Matsubara axis at 100 K. The effective mass enhancement  $m^*/m$  of Ni- $d_{z^2}$  and Ni- $d_{x^2-y^2}$  orbitals in inner and outer layers at 100 K as functions of (c) Hund's rule coupling  $J$  at  $U = 4$  eV and (d) Hubbard  $U$  at  $J = 0$  eV.

The effective mass enhancement  $m^*/m = 1/Z$  as functions of  $U$  and  $J$  at 100 K are plotted in Fig. 3 (c-d). To avoid a large error bar in the analytic continuation, we directly calculate the quasi-particle weight  $Z$  from the fourth-order polynomial fit to the self-energies at the first ten Matsubara frequencies. For  $U = 4$  eV and  $J = 0$  eV, the  $m^*/m$  of Ni- $d_{z^2}$  and Ni- $d_{x^2-y^2}$  orbitals in both inner and outer layers are similar.

And when  $J$  increased from 0 to 1 eV, the  $m^*/m$  of Ni- $d_{z^2}$  and Ni- $d_{x^2-y^2}$  orbitals in outer layers increases from 1.36 and 1.34 to 2.64 and 2.14, respectively, in which the increasing ratio are 1.94 and 1.6, respectively. While for the Ni- $d_{z^2}$  and Ni- $d_{x^2-y^2}$  orbitals in inner layers increases from 1.31 and 1.29 to 2.01 and 1.89, while the increasing ratio are 1.53 and 1.47. The magnitude of electronic correlation of Ni- $d$  electrons in outer layers are strong sensitivity on the Hund's rule coupling than these in inner layers. Besides, the difference of  $m^*/m$  between the Ni- $d_{z^2}$  and Ni- $d_{x^2-y^2}$

orbitals in outer layer are higher than in inner layers, indicating a strong orbital-dependent of these orbitals in outer layers. For  $J = 0$  eV, the  $m^*/m$  of Ni- $d_{z^2}$  and Ni- $d_{x^2-y^2}$  orbitals in outer layers increases from 1.15 and 1.13 to 1.6 and 1.55, respectively, and the increasing ratio for Ni- $d_{z^2}$  and Ni- $d_{x^2-y^2}$  orbitals are 1.39 and 1.37. For the Ni- $d_{z^2}$  and Ni- $d_{x^2-y^2}$  orbitals in inner layers increases from 1.13 and 1.12 to 1.51 and 1.48, corresponding with the increasing ratio for Ni- $d_{z^2}$  and Ni- $d_{x^2-y^2}$  orbitals at 1.34 and 1.32. Therefore, the evolution of  $m^*/m$  for these orbitals in both inner and outer layers indicate a weak sensitivity on the Hubbard  $U$ . It suggests that in  $\text{La}_4\text{Ni}_3\text{O}_{10}$  the Hund's rule coupling plays more important role in modulate the strength of electronic correlations than the Hubbard  $U$ .

Fig. 4(a) shows the evolution of instantaneous local magnetic moment  $M$  as a function of the temperature. The local magnetic moment can be expressed as  $M = 2\sqrt{\sum_k P_k S_k^{z^2}}$ , where  $P_k$  is the probability of atomic states. The local magnetic moment  $M$  in both inner and outer layers slightly increases when the temperature increased. And this phenomenon may cause by the antiferromagnetic spin correlations [65], which is arise from the interlayer superexchange coupling between two Ni- $d_{z^2}$  spins through the apical O- $p_z$  orbital. Besides, the local magnetic moment  $M$  at  $J = 1$  eV in both inner and outer layers are large than those at  $J = 0$  eV. Therefore, the Hund's rule coupling would induce extra high-spin states in the  $I4/mmm$  phase of  $\text{La}_4\text{Ni}_3\text{O}_{10}$ .

We also calculated the atomic spin state probability for the electron occupation number  $N = 7$  and 8 as a function of  $J$  in Fig. 4 (c-d). For  $J = 0$  eV, the maximum possibility atomic spin state is low-spin with  $N = 8$ ,  $S = 0$  in both inner and outer layers. It is worth to note that with the increment of  $J$ , the possibility of low-spin states with  $N = 8$ ,  $S = 0$  decreased and the high-spin states with  $N = 8$ ,  $S = 1$  increased. And when  $J$  is higher than 0.98 eV, the maximum possibility atomic spin state in inner layers is high-spin state with  $N = 8$ ,  $S = 1$ . For the outer layers, this transition starts when  $J$  is higher than 0.78 eV. Therefore, there is a competition between high-spin state and low-spin state in  $I4/mmm$  phase of  $\text{La}_4\text{Ni}_3\text{O}_{10}$ , which has also been suggested in infinite-layer nickelate [15, 66]. Since the atomic spin states are mainly controlled by the crystal field splitting if the Hund's rule coupling is not considered, the partition ratio between the high-spin states and the low-spin states may originate from the competition between Hund's rule coupling and the crystal field splitting. And the high-spin state induced by Hund's rule coupling would cause the orbital blocking effect [67], resulting an enhancement of the electronic correlation in  $I4/mmm$  phase of  $\text{La}_4\text{Ni}_3\text{O}_{10}$ . Besides, the transition value of  $J$  in inner layers are much larger than that in outer layers, which suggests a large crystal field splitting energy and a more itinerant nature in inner layers. We also calculated probability for the electron occupation number  $N = 7$  and  $N = 8$  as a function of Hund's rule coupling  $J$  for

*I4/mmm* phase of  $\text{La}_3\text{Ni}_2\text{O}_7$  at 30 GPa (the crystal structure was adopted from previous research [34]) and plotted the results in Fig. 4 (b). A similar phenomenon has also been found in *I4/mmm* phase of  $\text{La}_3\text{Ni}_2\text{O}_7$  with a transition value of  $J = 0.72$  eV, which is similar with that of outer layers and much lower than that of inner layers of *I4/mmm* phase of  $\text{La}_4\text{Ni}_3\text{O}_{10}$ . Since the hybridization between the  $\text{Ni}-d_{z^2}$  and  $\text{Ni}-d_{x^2-y^2}$  orbitals has been suggested to be important in the superconductivity in both  $\text{La}_3\text{Ni}_2\text{O}_7$  and  $\text{La}_4\text{Ni}_3\text{O}_{10}$  [42, 51, 68], a weak strength of Hund's rule in inner layers may not conducive for superconductivity and resulting a low  $T_c$  in pressured  $\text{La}_4\text{Ni}_3\text{O}_{10}$ .

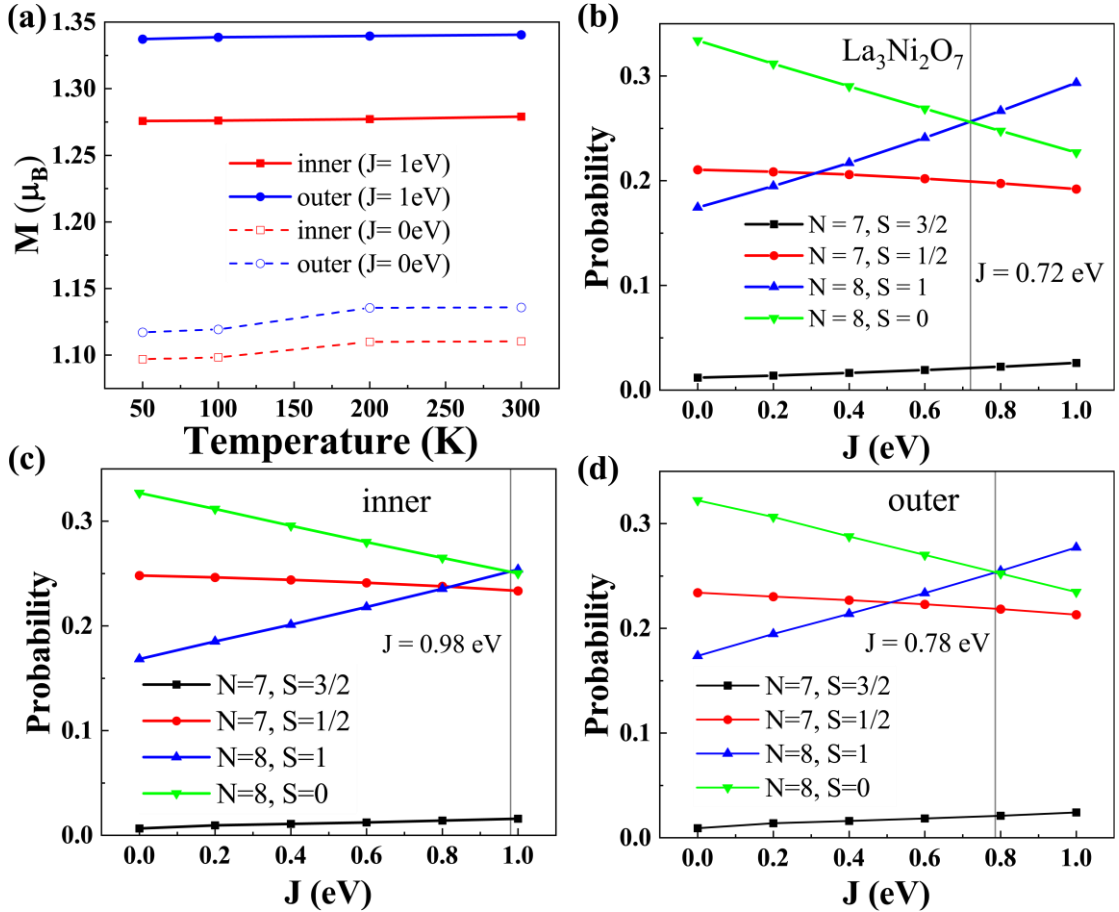


FIG 4. (a) Evolution of instantaneous local magnetic moment  $M$  as a function of the temperature with  $U = 4$  eV. Calculated probability for the electron occupation number  $N = 7$  and  $N = 8$  as a function of Hund's rule coupling  $J$  for (b) *I4/mmm*- $\text{La}_3\text{Ni}_2\text{O}_7$ , (c) inner layers, and (d) outer layers at 100 K.

#### IV. Conclusions

In summary, we performed a DFT+DMFT study on the effects of electronic correlations in  $\text{La}_4\text{Ni}_3\text{O}_{10}$  at both the ambient pressure and high pressure. Our calculated spectral functions and Fermi surface of the  $P2_1/a$  phase of  $\text{La}_4\text{Ni}_3\text{O}_{10}$  are nicely consistent with ARPES experimental results. By analyzing the self-energy functions and the quasi-particle weight, we found that the orbital-dependent and the layer-dependent feature in *I4/mmm* phase of  $\text{La}_4\text{Ni}_3\text{O}_{10}$  mainly originate from the Hund's rule coupling. Moreover, there existed a competition between the Hund's rule

coupling and the crystal field splitting, which controls the partitioning between the high-spin and the low-spin states in *I4/mmm* phase of  $\text{La}_4\text{Ni}_3\text{O}_{10}$ . The layer-dependent feature in *I4/mmm* phase of  $\text{La}_4\text{Ni}_3\text{O}_{10}$  is caused by the different crystal field splitting energy. Our study emphasize the importance of multi-orbital electronic correlations in trilayer nickelate  $\text{La}_4\text{Ni}_3\text{O}_{10}$  and can help understanding experimental results of this fancy superconducting compound.

## V. Acknowledgments

This work was supported by National Natural Science Foundation of China (Grants Nos. 12122405, 52072188 and 12274169), National Key R&D Program of China (Grants Nos. 2022YFA1402304 and 2023YFA1406200), Fundamental Research Funds for the Central Universities (Grants No. xzy022023011 and xhj032021014-04), and Program for Science and Technology Innovation Team in Zhejiang (Grant No. 2021R01004). Some of the calculations were performed at the High Performance Computing Center of Jilin University and using TianHe-1(A) at the National Supercomputer Center in Tianjin.

## VI. References

- [1] J. Bednorz and K. Müller, *Z. Phys. B Condens. Matter* **64**, 189 (1986).
- [2] M. Wu, J. Ashburn, C. Torng, P. Hor, R. Meng, L. Gao, Z. Huang, Y. Wang and C. Chu, *Phys. Rev. Lett.* **58**, 908 (1987).
- [3] P. Lee, N. Nagaosa and X. Wen, *Rev. Mod. Phys.* **78**, 17 (2006).
- [4] B. Keimer, S. Kivelson, M. Norman, S. Uchida and J. Zaanen, *Nature* **518**, 179 (2015).
- [5] V. Anisimov, D. Bakhvalov and T. Rice, *Phys. Rev. B* **59**, 7901 (1999).
- [6] K. Lee and W. Pickett, *Phys. Rev. B* **70**, 165109 (2004).
- [7] J. Chaloupka and G. Khaliullin, *Phys. Rev. Lett.* **100**, 016404 (2008).
- [8] J. Zhang, Y. Chen, D. Phelan, H. Zheng, M. Norman and J. Mitchell, *Proc. Natl. Acad. Sci. U.S.A.* **113**, 8945 (2016).
- [9] D. Li, K. Lee, B. Wang, M. Osada, S. Crossley, H. Lee, Y. Cui, Y. Hikita and H. Hwang, *Nature* **572**, 624 (2019).
- [10] M. Osada, B. Wang, B. Goodge, S. Harvey, K. Lee, D. Li, L. Kourkoutis and H. Hwang, *Adv. Mater.* **33**, 2104083 (2021).
- [11] N. Wang, M. Yang, Z. Yang, K. Chen, H. Zhang, Q. Zhang, Z. Zhu, Y. Uwatoko, L. Gu, X. Dong, J. Sun, K. Jin and J. Cheng, *Nat. Commun.* **13**, 4367 (2022).
- [12] W. Sun, Y. Li, R. Liu, J. Yang, J. Li, W. Wei, G. Jin, S. Yan, H. Sun, W. Guo, Z. Gu, Z. Zhu, Y. Sun, Z. Shi, Y. Deng, X. Wang and Y. Nie, *Adv. Mater.* **35**, 2303400 (2023).
- [13] D. Li, B. Wang, K. Lee, S. Harvey, M. Osada, B. Goodge, L. Kourkoutis and H. Hwang, *Phys. Rev. Lett.* **125**, 027001 (2020).
- [14] S. Zeng, C. Tang, X. Yin, C. Li, M. Li, Z. Huang, J. Hu, W. Liu, G. Omar, H. Jani, Z. Lim, K. Han, D. Wan, P. Yang, S. Pennycook, A. Wee and A. Ariando, *Phys. Rev. Lett.* **125**, 147003 (2020).

- [15] X. Wan, V. Ivanov, G. Resta, I. Leonov and S. Savrasov, Phys. Rev. B **103**, 075123 (2021).
- [16] Y. Wang, C. Kang, H. Miao and G. Kotliar, Phys. Rev. B **102**, 161118 (2020).
- [17] G. Zhang, Y. Yang and F. Zhang, Phys. Rev. B **101**, 020501 (2020).
- [18] M. Hepting, D. Li, C. Jia, H. Lu, E. Paris, Y. Tseng, X. Feng, M. Osada, E. Been, Y. Hikita, Y. Chuang, Z. Hussain, K. Zhou, A. Nag, M. Garcia-Fernandez, M. Rossi, H. Huang, D. Huang, Z. Shen, T. Schmitt, H. Hwang, B. Moritz, J. Zaanen, T. Devereaux and W. Lee, Nat. Mater. **19**, 381 (2020).
- [19] B. Goodge, D. Li, K. Lee, M. Osada, B. Wang, G. Sawatzky, H. Hwang and L. Kourkoutis, Proc. Natl. Acad. Sci. U.S.A. **118**, e2007683118 (2021).
- [20] H. Sun, M. Huo, X. Hu, J. Li, Z. Liu, Y. Han, L. Tang, Z. Mao, P. Yang, B. Wang, J. Cheng, D. Yao, G. Zhang and M. Wang, Nature **621**, 493 (2023).
- [21] J. Hou, P. Yang, Z. Liu, J. Li, P. Shan, L. Ma, G. Wang, N. Wang, H. Guo, J. Sun, Y. Uwatoko, M. Wang, G. Zhang, B. Wang and J. Cheng, Chin. Phys. Lett. **40**, 117302 (2023).
- [22] Y. Zhang, D. Su, Y. Huang, H. Sun, M. Huo, Z. Shan, K. Ye, Z. Yang, R. Li, M. Smidman, M. Wang, L. Jiao and H. Yuan, arXiv preprint arXiv:2307.14819 (2023).
- [23] Y. Zhou, J. Guo, S. Cai, H. Sun, P. Wang, J. Zhao, J. Han, X. Chen, Q. Wu, Y. Ding, M. Wang, T. Xiang, H. Mao and L. Sun, arxiv preprint arXiv:2311.12361 (2023).
- [24] G. Wang, N. Wang, X. Shen, J. Hou, L. Ma, L. Shi, Z. Ren, Y. Gu, H. Ma, P. Yang, Z. Liu, H. Guo, J. Sun, G. Zhang, S. Calder, J. Yan, B. Wang, Y. Uwatoko and J. Cheng, Phys. Rev. X **14**, 011040 (2024).
- [25] J. Li, P. Ma, H. Zhang, X. Huang, C. Huang, M. Huo, D. Hu, Z. Dong, C. He, J. Liao, X. Chen, T. Xie, H. Sun and M. Wang, arXiv preprint arXiv:2404.11369 (2024).
- [26] Z. Luo, X. Hu, M. Wang, W. Wú and D. Yao, Phys. Rev. Lett. **131**, 126001 (2023).
- [27] X. Qu, D. Qu, J. Chen, C. Wu, F. Yang, W. Li and G. Su, Phys. Rev. Lett. **132**, 036502 (2024).
- [28] D. Shilenko and I. Leonov, Phys. Rev. B **108**, 125105 (2023).
- [29] W. Wú, Z. Luo, D. Yao and M. Wang, Sci. China-Phys. Mech. **67**, 117402 (2024).
- [30] Y. Cao and Y. Yang, Phys. Rev. B **109**, L081105 (2024).
- [31] V. Christiansson, F. Petocchi and P. Werner, Phys. Rev. Lett. **131**, 206501 (2023).
- [32] F. Lechermann, J. Gondolf, S. Bötzeli and I. Eremin, Phys. Rev. B **108**, L201121 (2023).
- [33] Y. Zhang, L. Lin, A. Moreo and E. Dagotto, Phys. Rev. B **108**, L180510 (2023).
- [34] Z. Huo, P. Zhang, A. Yang, Z. Liu, X. Tao, Z. Zhang, Q. Jiang, W. Chen, D. Duan and T. Cui, arXiv preprint arXiv:2404.11001 (2024).
- [35] Y. Liu, J. Mei, F. Ye, W. Chen and F. Yang, Phys. Rev. Lett. **131**, 236002 (2023)
- [36] X. Chen, J. Choi, Z. Jiang, J. Mei, K. Jiang, J. Li, S. Agrestini, M. Garcia-Fernandez, X. Huang, H. Sun, D. Shen, M. Wang, J. Hu, Y. Lu, K. Zhou and D. Feng, arXiv preprint arXiv:2401.12657 (2024).

[37] J. Yang, H. Sun, X. Hu, Y. Xie, T. Miao, H. Luo, H. Chen, B. Liang, W. Zhu, G. Qu, C. Chen, M. Huo, Y. Huang, S. Zhang, F. Zhang, F. Yang, Z. Wang, Q. Peng, H. Mao, G. Liu, Z. Xu, T. Qian, D. Yao, M. Wang, L. Zhao and X. Zhou, *Nat. Commun.* **15**, 4373 (2024).

[38] J. Chen, F. Yang and W. Li, arXiv preprint arXiv:2311.05491 (2023).

[39] H. Oh and Y. Zhang, *Phys. Rev. B* **108**, 174511 (2023).

[40] X. Qu, D. Qu, W. Li and G. Su, arXiv preprint arXiv:2311.12769 (2023).

[41] C. Lu, Z. Pan, F. Yang and C. Wu, *Phys. Rev. Lett.* **132**, 146002 (2024).

[42] Y. Yang, G. Zhang and F. Zhang, *Phys. Rev. B* **108**, L201108 (2023).

[43] Y. Zhu, E. Zhang, B. Pan, X. Chen, D. Peng, L. Chen, H. Ren, F. Liu, N. Li, Z. Xing, J. Han, J. Wang, D. Jia, H. Wo, Y. Gu, Y. Gu, L. Ji, W. Wang, H. Guo, Y. Shen, T. Ying, X. Chen, W. Yang, C. Zheng, Q. Zeng, J. Guo and J. Zhao, arXiv preprint arXiv:2311.07353 (2023).

[44] J. Li, C. Chen, C. Huang, Y. Han, M. Huo, X. Huang, P. Ma, Z. Qiu, J. Chen, X. Hu, L. Chen, T. Xie, B. Shen, H. Sun, D. Yao and M. Wang, *Sci. China-Phys. Mech.* **67**, 117403 (2024).

[45] M. Zhang, C. Pei, X. Du, W. Hu, Y. Cao, Q. Wang, J. Wu, Y. Li, H. Liu, C. Wen, Y. Zhao, C. Li, W. Cao, S. Zhu, Q. Zhang, N. Yu, P. Cheng, L. Zhang, Z. Li, J. Zhao, Y. Chen, H. Guo, C. Wu, F. Yang, S. Yan, L. Yang and Y. Qi, arXiv preprint arXiv:2311.07423 (2023).

[46] Q. Li, Y. Zhang, Z. Xiang, Y. Zhang, X. Zhu and H. Wen, *Chin. Phys. Lett.* **41**, 017401 (2024).

[47] H. Sakakibara, M. Ochi, H. Nagata, Y. Ueki, H. Sakurai, R. Matsumoto, K. Terashima, K. Hirose, H. Ohta, M. Kato, Y. Takano and K. Kuroki, *Phys. Rev. B* **109**, 144511 (2024).

[48] X. Du, Y. Li, Y. Cao, C. Pei, M. Zhang, W. Zhao, K. Zhai, R. Xu, Z. Liu, Z. Li, J. Zhao, G. Li, Y. Chen, Y. Qi, H. Guo and L. Yang, arXiv preprint arXiv:2405.19853 (2024).

[49] M. Kakoi, T. Oi, Y. Ohshita, M. Yashima, K. Kuroki, T. Kato, H. Takahashi, S. Ishiwata, Y. Adachi, N. Hatada, T. Uda and H. Mukuda, *J. Phys. Soc. Jpn.* **93**, 053702 (2024).

[50] H. Oh, B. Zhou and Y. Zhang, arXiv preprint arXiv:2405.00092 (2024).

[51] Q. Qin, J. Wang and Y. Yang, arXiv preprint arXiv:2405.04340 (2024).

[52] Y. Zhang, L. Lin, A. Moreo, T. Maier and E. Dagotto, arXiv preprint arXiv:2402.05285 (2024).

[53] C. Chen, Z. Luo, M. Wang, W. Wu and D. Yao, arXiv preprint arXiv:2402.07196 (2024).

[54] Q. Yang, K. Jiang, D. Wang, H. Lu and Q. Wang, *Phys. Rev. B* **109**, L220506 (2024).

[55] J. Wang, Z. Ouyang, R. He and Z. Lu, *Phys. Rev. B* **109**, 165140 (2024).

[56] I. Leonov, *Phys. Rev. B* **109**, 235123 (2024).

[57] K. Haule, C. Yee and K. Kim, *Phys. Rev. B* **81**, 195107 (2010).

[58] P. Blaha, K. Schwarz, F. Tran, R. Laskowski, G. Madsen and L. Marks, *J. Chem. Phys.* **152**, 074101 (2020).

- [59] J. Perdew, K. Burke and M. Ernzerhof, Phys. Rev. Lett. **77**, 3865 (1996).
- [60] E. Gull, A. Millis, A. Lichtenstein, A. Rubtsov, M. Troyer and P. Werner, Rev. Mod. Phys. **83** (2), 349-404 (2011).
- [61] P. Werner, A. Comanac, L. Medici, M. Troyer and A. Millis, Phys. Rev. Lett. **97**, 076405 (2006).
- [62] K. Haule, Phys. Rev. B **75**, 155113 (2007).
- [63] A. Georges, G. Kotliar, W. Krauth and M. Rozenberg, Rev. Mod. Phys. **68**, 13 (1996).
- [64] M. Jarrell and J. Gubernatis, Phys. Rep. **269**, 133 (1996).
- [65] H. LaBollita, J. Kapeghian, M. Norman and A. Botana, Phys. Rev. B **109**, 195151 (2024).
- [66] Q. Gu and H. Wen, The Innovation **3**, 100202 (2022).
- [67] Z. Yin, K. Haule and G. Kotliar, Nat. Mater. **10**, 932 (2011).
- [68] M. Kakoi, T. Kaneko, H. Sakakibara, M. Ochi and K. Kuroki, Phys. Rev. B **109**, L201124 (2024).